ARTICLE

On-surface condensation of low-dimensional benzotriazole – copper assemblies†

Received 00th January 20xx,
Accepted 00th January 20xx

DOI: 10.1039/x0xx00000x

Federico Grillo,*[a] David Batchelor,[b] Christian R Larrea,[a] Stephen M Francis,[a] Paolo Lacovig,[c] and Neville V Richardson[a]

The reactivity of benzotriazole with copper on a gold surface has been studied by a combination of surface sensitive methods with support from DFT (density functional theory) calculations. For some time benzotriazole has been known to enhance the corrosion resistance of copper at the monolayer level, although the exact mechanism is still a matter of discussion and disagreement in the literature. A single crystal Au(111) surface allows to evaluate the interaction of weakly physisorbed, intact benzotriazole molecules with copper atoms dosed to sub-monolayer amounts. These interactions have been characterised, in the temperature range ca. 300 – 650 K, by scanning tunnelling microscopy, high resolution electron energy loss spectroscopy and synchrotron-based X-ray photoemission spectroscopy and near-edged X-ray absorption fine structure studies. Supporting DFT calculations considered the stability of isolated, gas-phase, benzotriazole/Cu species and their corresponding spectroscopic signature at the N K absorption edge. In agreement with previous investigations, benzotriazole physisorbs on a clean Au(111) surface at room temperature forming a hydrogen-bonded network of flat-lying BTAH molecules, relatively weakly bonded to the underlying gold surface. However, in the presence of co-adsorbed copper atoms, proton removal from the molecules leads to species better described as BTA^- interacting directly with Cu atoms. In these situations the molecules adopt a more upright orientation and $Cu(BTA)_2$ and -$[Cu(BTA)]_n$- species are formed, depending on temperature and coverage of the adsorbed species. These species are stable to relatively high temperatures, 550 – 600 K.

1. Introduction

The search for efficient and economical methods to protect metals and alloys from corrosion is a key aspect of industrial manufacturing. A well-known corrosion inhibitor for copper and copper alloys is benzotriazole (BTAH, scheme 1a); however, to date there is no universal consensus on either BTAH coordination mode with copper or its adsorption and passivation mechanism [1-4]. On the one hand, it is generally accepted that the ability of BTAH to act as an etching and corrosion inhibitor in aqueous media is attributed to the formation of strongly bound Cu-BTA surface complexes [5] (BTA is deprotonated BTAH). These may act as a water repellent physical barrier that impedes the adsorption of water and other polar organic molecules, conferring some degree of surface passivation [5, 6]. On the other hand, it has also been proposed that the passivating film comprises a hybrid hydrogen-bonded network enclosing some sections of a Cu(I)-BTA polymeric layer with a 1:1 Cu:BTA stoichiometry and a bidentate structure [5, 6]. However, there is still a lack of a clear experimental evidence regarding the morphology and chemical behaviour of these species. In fact, a variety of complex structures have been identified for the interaction of benzotriazole with different substrates at different temperatures and coverages [1-23]. In an ultra-high vacuum (UHV) environment, upon adsorption on reactive surfaces, benzotraizole has been shown to dissociate into BTA and hydrogen and chemisorb through the triazo moiety. Several ordered structures have been identified, including upright Cu(BTA) monomers [9-11, 19-20], $Cu(BTA)_2$ species (scheme 1b) [9-11], flat-lying [12-13, 20] or upright metal organic chains [11], in some cases stabilized by intramolecular hydrogen bonding [21].

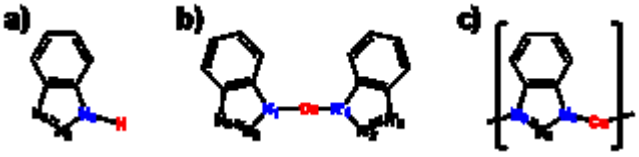

Scheme 1. Chemical structures of: a) BTAH; b) a $Cu(BTA)_2$ species; c) $-[CuBTA]_n-$ monomer of the "necklace" polymer. Nitrogen atoms are labelled for ease of description and discussion.

[a] *EaStCHEM - School of Chemistry, University of St. Andrews, St. Andrews, KY16 9ST, United Kingdom. e-mail: federico.grillo@st-andrews.ac.uk*
[b] *Karlsruhe Institut für Technologie (KIT)- IPS, Hermann-von-Helmholtz-Platz 1, 76344 Eggenstein, Deutschland*
[c] *Elettra – Sinctrotrone Trieste, S.C.p.A., S.S. 14 km 163.5, 34149 Basovizza, Trieste, Italy.*

†Electronic Supplementary Information (ESI) available: additional STM images, NEXAFS on Au(111), NEXAFS on Cu/Au(111), optimised geometries, N-K calculated excitation energies. See DOI: 10.1039/x0xx00000x

Computational works have considered various adsorption configurations including physisorption as a flat-lying molecule [2, 4, 6, 22], formation of hydrogen-bonded overlayers [3, 8, 11], chemisorption as an intact molecule through the triazole moiety [2, 4, 6, 22], or through deprotonation and formation of structures stabilized by copper surface atoms [3, 8, 11, 15, 23]. Metal organic Cu-BTA complexes such as chmisorbed $Cu(BTA)_2$ species [7-8, 11, 15], or $–[Cu(BTA)]_n–$ chains, the so-called "necklace" polymer (scheme 1c) [3, 7-8, 11, 15, 22-23] have also been considered. Even though $–[Cu(BTA)]_n–$ chains adsorbed with a BTA unit upright and adjacent units tilted to a variable angle with respect to the surface normal represent the theoretically most energetically favored structures [3, 8, 11], upright $Cu(BTA)_2$ species [9, 10] or a combination of both have been reported experimentally [11].

Additionally, the specific adsorption sites present on a surface directly relate to the morphology of the substrates. On a metallic substrate, an adsorption site may change its configuration because of the presence of adatoms [8, 11, 24, 25]. The role of copper adatoms in influencing the adsorption morphology on Cu(111) has been recently considered [3, 8, 11, 15, 23]; the authors concluded that the adsorbed structures are a combination of variable amounts of metal organic Cu-BTA structures including $–[Cu(BTA)]_n–$ polymeric chains and $Cu(BTA)_2$ species adsorbed at various orientations [11].

An alternative way to investigate the role of mobile copper atoms is to consider the interaction between benzotriazole and copper on a less reactive substrate, for example Au(111). This stems from the observation that BTAH preferentially chemisorbs over reactive substrates [9, 10, 12, 13, 18-21] and physisorbs over unreactive ones [14]. Moreover, the determination of the oxidation state of the copper atoms embedded in the organic matrix can be extremely difficult when the experiments are carried out using a copper surface as a substrate, as recently demonstrated [11].

In this work, to gain a better understanding of the chemistry of benzotriazole and its binding with copper, BTAH was dosed on copper-doped Au(111) surfaces. On such a substrate, Au(111) merely acts as a 2D inert support and copper-rich islands formed on the Au(111) crystal surface [26, 27] can be regarded as a reservoir of copper atoms [28-33], which react with BTAH to form low-dimensional metal organic species. Combined scanning tunnelling microscopy (STM), high resolution electron energy loss spectroscopy (HREELS), photoemission spectroscopy (PES), near-edge X-ray absorption fine structure (NEXAFS) and density functional theory (DFT) calculations allowed us to derive adsorption models to gain a better understanding of the morphology, composition and thermal stability of the adsorbed structures, and the selectivity of benzotriazole for copper.

2. Results and discussion

2.1 Experimental

2.1.1 Scanning tunnelling microscopy

Copper has been shown to nucleate at the elbows of the clean Au(111) (22 × √3) reconstruction [26, 27]. At increased coverage, ca. 0.2 ML (monolayer), copper-rich islands of characteristic 'D' shape form via a substrate templating effect. Small copper clusters can still be observed at some elbows; step edges are also decorated. Copper-rich islands are characterised by regular and straight edges and a surface with discommensuration lines reminiscent of the herringbone reconstruction.

On these surfaces, BTAH physisorbs on the unmodified Au(111) regions and chemisorbs on copper-rich areas, figure 1a. Namely, BTAH selectively chemisorbs at the elbows of the herringbone reconstruction, i and inset in figure 1a, on copper-rich islands, ii in figure 1a, and at copper decorated step edges, iii in figure 1a. It is worth noting that STM is unable to image the physisorbed species at room temperature because of fast diffusion [14].

Molecules assemble in small ensembles at the elbows of the herringbone reconstruction. These structures correspond to $Cu_x(BTA)_y$ metallorganic complexes, as will be further corroborated in the discussion of the spectroscopic data. They are characterised by central brighter features of elongated shape, having a lateral separation of around 0.42 nm (line profile *a* in figure 1e), surrounded by dimmer and slightly more rounded features (apparent heights are ca. 1 Å and ca. 0.55 Å respectively, line profiles *b* and *a* in figure 1e, respectively). Each of these features is attributed to benzotriazolate molecules nucleated at, and coordinating to a small Cu_n cluster. The difference in apparent heights suggests that brighter features represent upright molecules, whereas dimmer features are attributed to molecules orientated with their molecular plane more parallel to the surface. Such molecular ensembles may find correspondence with Cu-BTA clusters produced in solution, one of which was modelled as $Cu_6(BTA)_4$, having a tetrahedral Cu_4 core, surrounded by two BTA-Cu(I)-BTA units [34]. In the present case, the observed ensembles may result from a combination of these, or similar clusters, adsorbed on the Au(111) surface. $Cu_x(BTA)_y$ ensembles do not appear to populate every elbow of the herringbone reconstruction, figure SI1. Moreover, the directions of their elongations are not random but rather seem to be related to the orientation of the elbows and to align with the close packed directions of the underlying Au(111). Adjacent ensembles do not necessarily exhibit elongation in the same direction, as neighbours may grow towards the same or the opposite side of the elbow.

On copper-rich islands, ii in figure 1a, and figure SI2, which have an apparent height of ca. 1.85 Å (line profile *c* in figure 1f), $Cu_x(BTA)_y$ species are adsorbed in a less ordered fashion than those at the herringbone elbows. A higher concentration of ensembles is seen at the ridges of the discommensuration lines over the islands; these are highly stressed, strained areas, and correspondingly more reactive [35].

ARTICLE

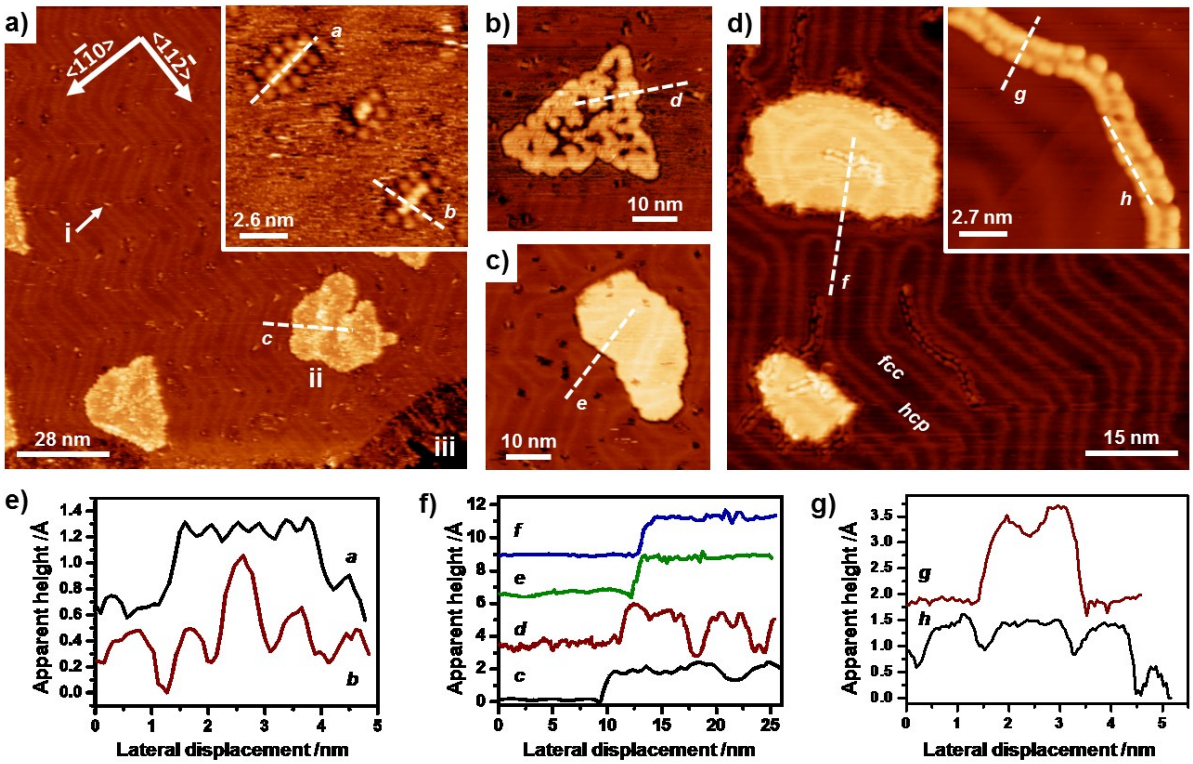

Fig. 1 a) STM images showing the features produced upon deposition of BTAH to nominal saturation on ca. 0.2 ML (monolayer) Cu/Au(111). a) room temperature; i indicates $Cu_x(BTA)_y$ species nucleated at herringbone elbows, ii indicates condensation on a Cu-rich island, iii indicates condensation at a Cu-rich step-edge; 140 × 140 nm^2, -1.2 V, 0.2 nA; inset) 13 × 13 nm^2, -1 V, 0.1 nA; b) annealing to ca. 400 K, 50 × 50 nm^2, -1.5 V, 1.0 nA; c) annealing to ca. 450 K, 50 × 50 nm^2, -1.5 V, 0.2 nA; d) annealing to ca. 500 K, 75 × 75 nm^2, -1.2 V, 0.1 nA; inset) 13.5 × 13.5 nm^2, -1.2 V, 0.04 nA; e) line profiles as in the inset in a); f) line profiles for copper-rich islands as in a), b), c) and d); g) line profiles as in the inset in d).

An added complexity is that the top layers of Cu-doped Au(111) surfaces are generally intermixed [26-29, 32], therefore benzotriazole can not only react with copper adatoms, but also with copper atoms within the surface plane. Features observed at the edges of the islands (figure SI2) may correspond to a line of single molecules. Similarly, molecular features typically follow and have an elongation normal to the step edge, at copper-decorated gold step edges (figure 1a, iii and also figures SI1, SI2, SI3).

Upon heating these preparations to progressively higher temperatures (400 K), weakly bound hydrogen-bonded species desorb. Copper-rich islands, formerly covered by a disordered $Cu_x(BTA)_y$, undergo an etching process, as displayed in figure 1b and by the line profile *d* in figure 1f, which shows an apparent height of ca. 1.9 Å, with some depressions having the same height. This is ascribed to the combination of two different phenomena. On the one hand, $Cu_x(BTA)_y$ weakly bound to the gold surface desorbs from copper-rich islands. In fact, the formation of the $Cu_x(BTA)_y$ species may result in the weakening of the interaction between the copper atoms and the Au(111) surface. As a comparison, in the case of the adsorption of BTAH on Cu(111), temperature programmed desorption measurements show that a saturated monolayer is stable up to ca. 600 K, whereas the physisorbed layer is seen to desorb at ca. 400 K. The chemisorbed layer is thought to desorb in the form of $Cu_x(BTA)_y$ [10, 34]. On the other hand, in Cu-doped Au(111) systems, copper has the tendency to diffuse into the bulk gold upon annealing [27, 28, 32].

In figure 1c features recorded after annealing to ca. 450 K are shown. The topography of the surface is almost restored to that of a clean preparation following the annealing step, except for the ragged appearance of the step edges, a clear consequence of the etching process. Nevertheless the islands appear clean and flat, with a measured step height of ca. 2.2 Å (line profile *e* in figure 1f), a value in good agreement with that of clean Au(111) [26, 27, 29], as if the etching were healed. A few

$Cu_x(BTA)_y$ ensembles are still visible at the elbows of the discommensuration lines. Island peripheries and step edges are cleaner, yet decorated by a single line of molecular features.

Features adsorbed at the elbows of the herringbone reconstruction are stable up to ca. 500 K, when the formation of a new structure is seen, as shown in figure 1d and inset. Such new features originate at the edges of copper-rich islands, or at gold step edges, and grow toward the terraces. These features are thought to be formed by $Cu_x(BTA)_y$ sub-units and are confined within the herringbone ridges. They are mostly localised on the *fcc* regions of the surface, seldom crossing over the bridge sites into the *hcp* areas. Such structures have an apparent height of ca. 1.6 Å and a width of *ca*. 2 nm (line profile *g* in figure 1g). Some sub-unit have a length of ca. 1.2 nm, which could correspond to a $Cu(BTA)_2$ species [9]; some other sub-units have a length of ca. 1.6 nm (line profile *h* in figure 1g); some portions are not resolved enough to determine the periodicity. As for the $Cu_x(BTA)_y$ ensembles observed at the elbows of the herringbone reconstruction upon BTAH dosage (figure 1a), such features have similarities with a recently synthesized polymorph comprising three crystallographically independent Cu(I) ions and two BTA ligands. These form a $[Cu_2(BTA)_2]$ sub-unit, which aligns in an antiparallel fashion to form a $[Cu_2(BTA)_2]_2$ secondary building unit, further linked through bridging Cu(I) atoms, resulting in a one-dimensional chain structure along the *c* axis [36]. Apart from the presence of such structures, the islands remain largely flat and clean, presumably gold-terminated, and exhibit a step height of ca. 2.25 Å (line profile *f* in figure 1f).

2.1.2 High resolution electron energy loss spectroscopy

After exposing the Cu-doped Au(111) surface to BTAH to saturation, the vibrational spectrum at room temperature (figure 2a) is dominated by the energy loss signals generated by flat-lying hydrogen-bonded interlocked species, as it shows the same peaks recorded on clean Au(111) [14]. The observed energy losses and their assignments are summarised in table 1. As already highlighted, such species are not imaged via STM because of fast diffusion across the surface, however their energy losses can be recorded via HREELS. Energy losses are observed at 270 cm^{-1} corresponding to an out-of-plane buckling mode of the full molecule, 425 cm^{-1} (with a shoulder at 525 cm^{-1}) due to 6- and 5- member rings out-of-plane deformations, 750 cm^{-1} assigned to the C-H out-of-plane bending mode, with a very weak shoulder at ca. 690 cm^{-1} due to the N_1-H out-of-plane bending mode and a weak 3055 cm^{-1} C-H stretching mode. The absence of the N_1-H stretch, expected at ca. 3500 cm^{-1} [37], confirms flat adsorption. Weak C-N and C-C in-plane related vibrations for the flat molecule, or for a more upright species, account for a raised background in the range 1000 – 1500 cm^{-1}. The vibrations generated by the physisorbed hydrogen-bonded species mask those generated by the chemisorbed species, which represent a minority of the adsorbed species and are related to the amount of copper dosed.

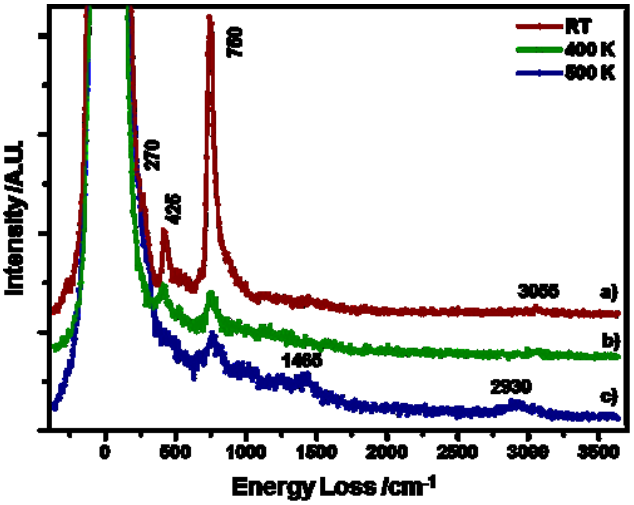

Fig. 2. HREEL spectra following dosing of Cu (ca. 20%) and BTAH (to saturation) as prepared at room temperature (a) and after annealing to 400 K (b) and 500 K (c).

Table 1. Observed energy losses and assignments /cm^{-1}

mode	RT	400 K	500 K	Ref.
ν CH	3055	3055	3055, 2930	9,10, 14, 38-40
ν C_6H_4 ring			1465	9,10, 38-40
ν NNN in N---Cu(I)			1250	10, 34
ν NNN + ν CH			1150	9, 38-42
δ CH			985	9,10, 38, 39, 41
γ CH	750	755	760	10, 14, 38, 42
γ NH	680			14,
oop C_6H_4 ring	530	525	520	10, 14
oop C_6H_4 ring	425	400		10, 14
whole molecule buckling	270	270		14

ν stretch, δ in-plane bend, γ out-of-plane (oop) bend

With annealing, the desorption of the physisorbed flat-lying species and concomitant decrease in their spectral finger print, opens up the possibility to record the signals pertaining to the chemisorbed species. In fact, the spectrum seen after annealing to 400 K, figure 2b, is related to the species observed at herringbone elbows and to those condensed at step edges, which are likely orientated in a more tilted geometry. After annealing the energy loss peaks related to the more upright species become more intense (500 K, figure 2c).

This spectrum is a summation of vibrations generated predominantly by upright and, to a lesser extent, flat-lying species coordinated with copper atoms. In particular, the intensities of the out-of-plane vibrations at 270 cm^{-1} and 400 cm^{-1} are less intense; the CH out-of-plane bend mode at 750 cm^{-1} shows the more important attenuation, due to both desorption of the hydrogen-bonded species and partial re-orientation of the remaining molecules upon reaction with the copper atoms. Correspondingly, the CH in-plane wagging mode

accounts for a raised background at around 1000 cm^{-1}; the small peaks at ca. 1150 and 1250 cm^{-1} are assigned to in-plane N-N stretches of the triazole ring in a Cu(I)---N configuration [10, 34]; the vibration at 1465 cm^{-1} is assigned to in-plane vibrational modes of the aromatic C_6H_4 rings, and the peaks at 2930 cm^{-1} and shoulder 3055 cm^{-1} are assigned to CH stretches.

2.1.3 Photoemission

Figure 3 shows photoemission spectra following dosing of copper to ca. 0.2 ML and BTAH to saturation on the Au(111) surface and annealing steps. The as prepared Cu $2p_{3/2}$ peak is recorded at 932.6 eV (full width at half maximum, fwhm, 0.92 eV), indicating that following adsorption on the clean Au(111) surface copper is in its metallic oxidation state (figure 3, left panel b) [43, 44, 45]. After exposure to BTAH the Cu $2p_{3/2}$ peak shifts to 932.2 eV (figure 3, left panel c), and there is a small increase of the fwhm to 0.98 eV. This indicates that the electronic configuration of metallic copper is modified by the interaction with benzotriazole, in favour of a more oxidised copper species. A clear assignment to copper in the +1 oxidation state is complicated since the binding energies for Cu(0) and Cu(I) fall roughly within the same range [43-45]. Furthermore, copper and gold can alloy and are completely miscible over a wide temperature range. Thus, the concentration of copper atoms in the uppermost gold layers, their chemical environments [27, l29, 32] and binding energies will vary [46-48]. Therefore, an unequivocal assignment to a specific copper species in a specific position or chemical state, i.e. in the surface layer, on the surface, or adatoms, is here not feasible. Nevertheless, a clear binding energy downshift is seen upon exposure to BTAH. On clean Cu(111), copper adatoms are predicted to show a downshift in binding energy with respect to bulk copper, whereas the shift in binding energy for copper atoms coordinated to BTAH has been calculated to span within 1.5-2 eV; the direction and magnitude of the shifts depend upon the specific N-Cu environment [11]. The absence of signals at higher binding energy values rules out the presence of Cu (II) [43-45]. The overall peak position stays constant up to annealing to 500 K. By 670 K the signal completely vanishes, confirming once more that copper has either desorbed as a $Cu_x(BTA)_y$ compound, dissolved into the bulk gold, or more likely a combination of both, as also supported by the STM measurements.

After exposure to BTAH, the N 1s region shows a signal which is best fitted with three components with maxima at 399.3, 400.2 and 400.6 eV (fwhm 0.85 eV) and area ratio ca. 1:1:2 (figure 3, central panel) .

Similar binding energies were recorded for BTAH dosed to yield saturation on Cu(111) [11]. Upon adsorption on pristine Au(111), only two peaks were reported, at 400.4 and 399.4 eV; these were assigned to the two inequivalent nitrogen atoms expected for hydrogen-bonded structures [14]. The observation of a doublet is also consistent with measurements on solid pellets of benzotriazole [49]. The triplet measured upon preparation may derive from the combination of flat-lying hydrogen-bonded species and deprotonated species of various structures. A comparison with binding energies values recorded on different systems is reported in table 2.

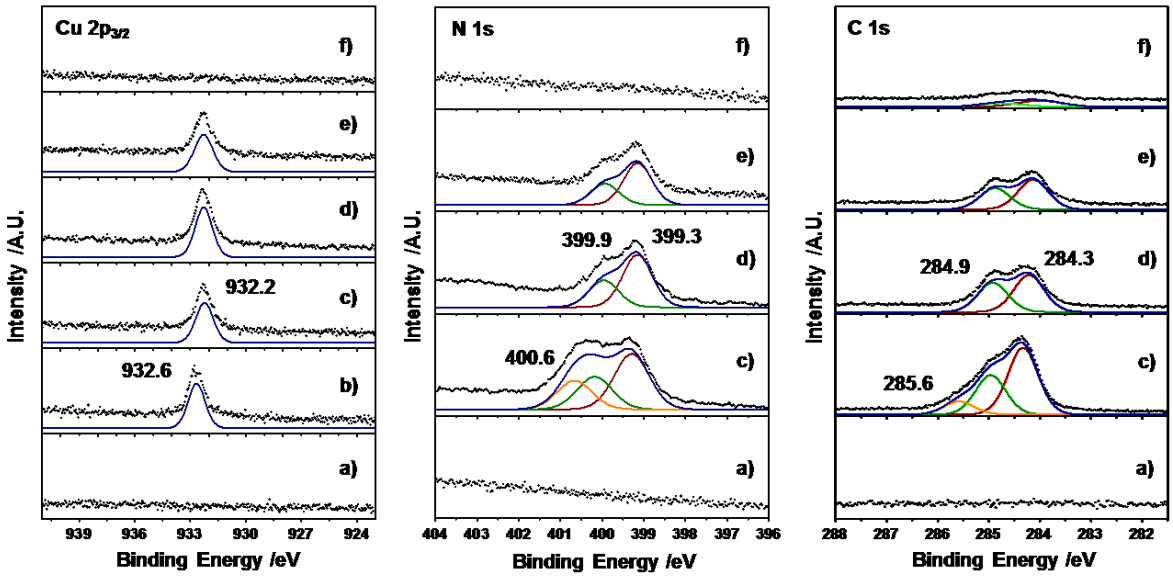

Fig. 3. Cu $2p_{3/2}$, N 1s and C 1s photoemission spectra following dosing of Cu (ca. 20%) and BTAH (to saturation) on the Au(111) surface as prepared at room temperature and after annealing; a) clean Au(111); b) copper dose; c) BTAH dose; d) anneal to 400 K; e) anneal to 500 K; f) anneal to 670 K. Data points in black; fits in colours.

Table 2. N 1s binding energy values; comparison with literature

Species	BE /eV	Ref.
BTAH/Cu/Au(111)	399.3 400.2 400.6 (as prep) 399.3 399.9 (anneal) 399.4 400.3 (low θ)	*This work*
BTAH /Cu(111)	399.2 400.2 401.3 (high θ)	11
BTAH Au(111)	399.4 400.4	14
BTA(H?)/Cu wafer	399.9	42
BTA(H?) pellet	399.5 N-N*-N 400.5 N-N*-C	
Cu(II)BTA	399.8	49
BTA(H_2O) / Cu	399.8	50
Cu^0BTAH $Cu^+(BTA)^-$ $Cu^{2+}(BTA^-)_2$	400.0	51
5Cl-BTA / Ni	400.8	52
BTA(H_2O)/NaCl/Cu	400.5 398.5 (sputter)	53
NaBTA solid	399.9	*This work*

θ coverage

Table 3: Changes in photoemission signals with temperature

temp /K	Cu $2p_{3/2}$ /%	N 1s /%	C 1s /%	N:C	Cu:BTA	notes
RT	100					Cu dosed on Au(111)
RT	94	100	100	1:2.5	1:1	BTAH dosed on Cu/Au(111)
400	115	57	55.6	1:2.45	1:0.44	ΔCu +21%; ΔN -43%; ΔC -44.4%
500	92	42.75	42.8	1:2.5	1:0.42	ΔCu -23%; ΔN -14.3%; ΔC -12.8%
670	-		12.6	-	-	molecular desorption complete

After annealing to 400 K the peak at higher binding energy disappears, the one at 400.2 eV shifts to 399.9 eV but stays in a 1:2 ratio with the component at 399.3 eV. Such an intensity ratio is the opposite of that recorded on Au(111). This implies a coordination different from hydrogen bonding and more in favour of metal organic compounds in which BTA is associated to Cu(I) [34, 36], well in agreement with the STM observations. Such a doublet in the N 1s core level region was previously associated with either BTA monomers bound to adatoms via both the N_1 and N_3 atoms in a bidentate configuration, or with a low coverage of -[CuBTA]$_n$- chains [11]. After annealing to 500 K the remaining peaks decrease in intensity, but their ratios stay constant. The signal disappears upon annealing to 670 K.

The C 1s region shows a signal which is best fitted with three components having binding energy of 285.6 eV, 284.9 eV and 284.3 eV (fwhm 0.6 eV) and area ratio 0.33:1:1.7 (figure 3, right t panel). By comparison, a single C 1s peak at 284.8 eV, with an asymmetry towards higher binding energies, was recorded on Cu(111) [11]. On Au(111), a doublet with maxima at 285.3 eV and 284.3 eV (area ratio 1:2.2) was recorded [14].

After annealing to 400 K, the peak at 285.6 eV is lost; the other two decrease in intensity and have a 1:1.4 area ratio, suggesting that the benzene rings are in slightly different chemical environments than on Au(111). After annealing to 673 K, some residual carbonaceous species are present, which cannot be removed by further annealing, only by sputtering.

A N:C ratio of 1:2.5 was derived from the PES data, versus the expected stoichiometric 1:2 ratio, which remains approximately constant throughout the annealing treatments (1:2.45 at 400 K, 1:2.5 at 500 K), indicating that the BTA moiety in $Cu_x(BTA)_y$ is stable up to at least 500 K. The Cu:BTA ratio is calculated as ca. 1:1 after preparation, 1:0.44 at 400 K and 1:0.42 at 500 K. Given that copper is in excess, the Cu:BTA ratio indicates that a portion of the copper atoms has coordinated to benzotriazole, and a portion has remained in, or close to, the Au(111) surface. As already highlighted, the Cu $2p_{3/2}$ core level signal includes multiple contributions, which are hardly distinguishable. The changes in the intensities of the photoemission signals are summarised in table 3.

2.1.4 Near edge X-ray absorption fine structure

Figure 4 shows angular dependent N K-edge NEXAFS spectra as prepared a) at room temperature, b) annealed to 400 K and c) to 500 K with d) the 90°-20° difference spectra at each temperature.

Spectra collected at room temperature, with reference to the one recorded at 20° in figure 4a, show π* resonances with maxima at 399.2, 400.0, 401.5 and 402.6 eV and σ* resonances at 407.2 and 412.0 eV. The peaks positions remain within ± 0.1 eV through the different angles recorded, except for the first σ* resonance, which progressively shifts to 406.9 eV. They are similar to those following adsorption on the pristine Au(111) surface [14] figure SI4a, albeit with two main differences: the fine structure in the π* resonance is not as resolved as on Au(111) and the dichroism is reduced, as evidenced by the presence of an appreciable π* resonance throughout the whole

range of angles recorded and shown by the 90°-20° spectra in figure 4d. The decrease in dichroism can be interpreted either as a change in the adsorption configuration of a single species from a flat-lying to a more tilted geometry, or as the presence of a mixture of flat-lying and upright species. Assuming a single species, an average tilt angle of 38° ± 5° for the triazole ring with respect to the surface was calculated (figure SI5a). As a comparison, an average tilt angle of 5° ± 3° was estimated following adsorption on Au(111) (figure SI4c).

The spectra recorded after annealing to 400 K, with reference to that measured at 20° in figure 4b, show a π* fine structure with resonances having maxima at 399.4, 400.0, 401.5 and 402.5 eV and σ* resonances at 407.1 and 411.8 eV. The main differences with respect to the as prepared spectrum are the relative increase in intensity of the resonance at 399.4 eV, and decrease of the resonances at 400.0 eV and 402.5 eV. Assuming the presence of a single molecular species, the average tilt angle is estimated as 44° ± 5° (figure SI5b).

After further annealing to 500 K (figure 1c), the NEXAFS signature remains very similar to that recorded at 400 K, with a further small loss in intensity. With reference to the spectrum recorded at 20°, π* resonances have maxima at 399.3, 399.9, 401.6, 403.1 and 405.0 eV and σ* resonances at 407.0 and 411.8 eV are recorded. Assuming a single molecular species, the calculated average angle of the triazole ring with respect to the surface is 40° ± 5° (figure SI5c).

2.2 Computational

Figure 5 shows calculated NEXAFS spectra at the N-edge for several "gas-phase" benzotriazole, and benzotriazole-copper, related species. Two geometrical configurations between a photon beam and a surface are considered. In grazing geometry (θ = 20°, red spectra) the incident beam is almost parallel to the surface and the electric field vector is close to the surface normal. In the normal geometry (θ = 90°, brown spectra) the incident direction is along the surface normal, with the electric vector parallel to the surface.

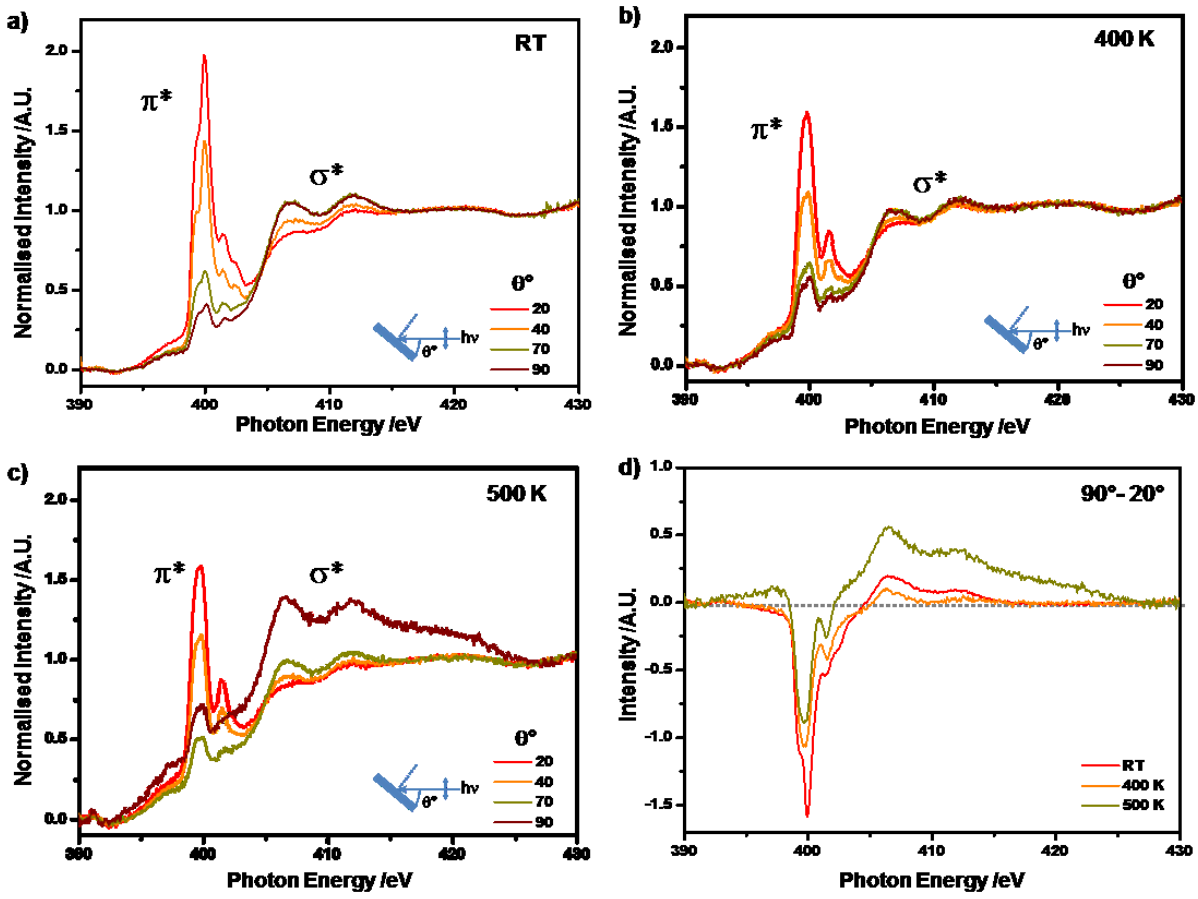

Fig. 4. N K-edge angular dependent NEXAFS spectra of a) as prepared saturated BTAH layer on 0.2 ML Cu/Au(111) at room temperature, b) after annealing to 400 K, c) to 500 K, d) 90°-20° spectra show opposite dichroism for both π* and σ* transitions at each temperature.

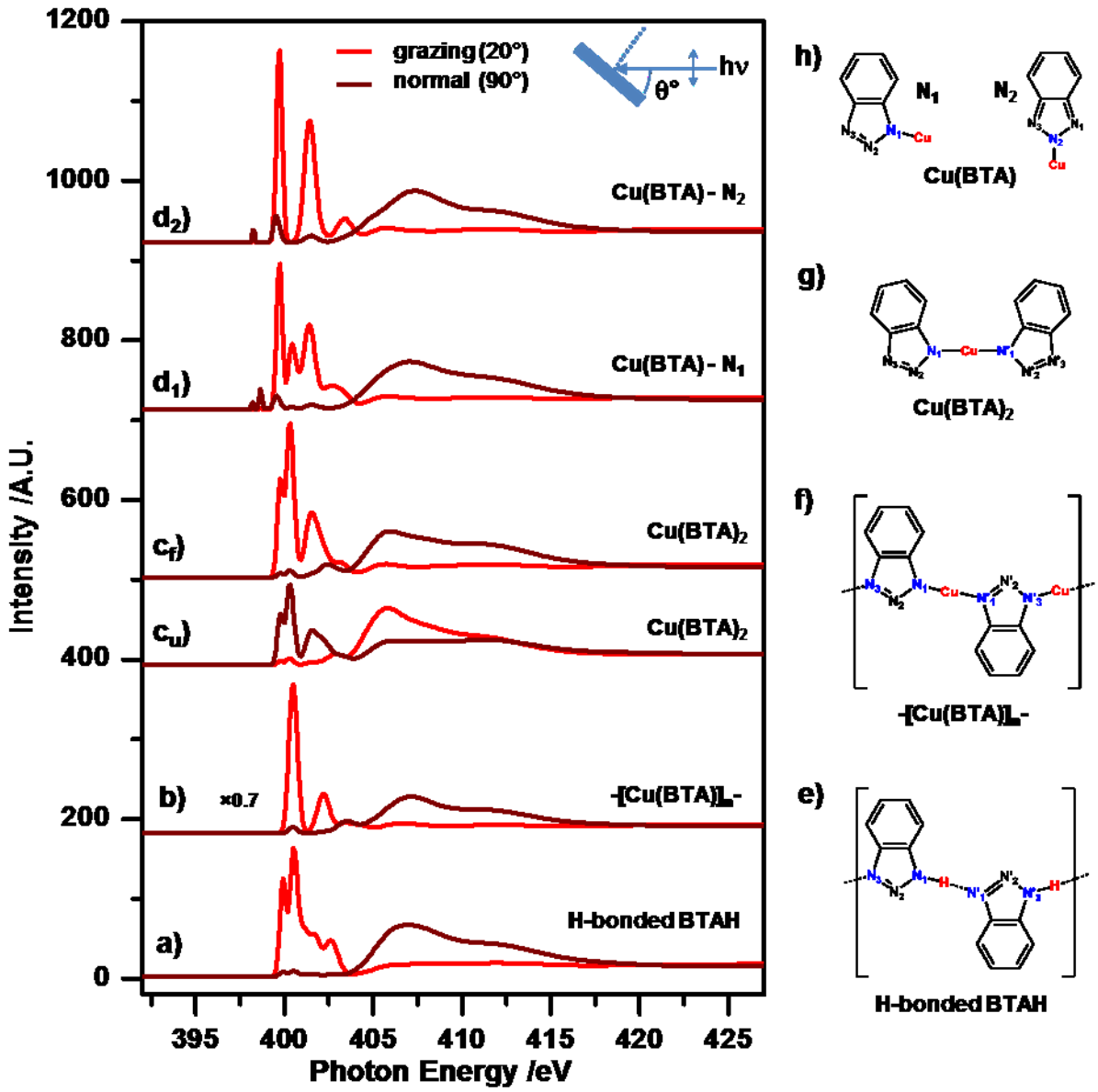

Fig. 5. N K-edge calculated NEXAFS spectra at normal (θ = 90°, brown spectra) and grazing incidence (θ = 20°, red spectra) for a) hydrogen-bonded BTAH chain, b) –[Cu(BTA)]$_n$– chain, c) Cu(BTA)$_2$ for both upright (c_u) and flat-lying (c_f) orientations, d) N_1 and N_2 Cu(BTA); e) – h) chemical structures corresponding to the calculated spectra in a) – d) respectively. Nitrogen atoms are numbered for ease of description and discussion.

Separate calculations considered the excitations induced by the electric vector of the photons aligned with the three distinct directions of these planar species, e.g. perpendicular to the plane, parallel to the long axis, and parallel to short axis of a given molecular species. Appropriate combinations of the spectra for these three orientations of the electric vector allow spectra for all possible surface orientations to be determined under any photon incidence angle. The threefold symmetry of the substrate allows the influence of the various molecular azimuthal orientations to be considered simply as a sum of the spectra of the relevant in-plane electric vector (*x,y*) components [54, 55]. In general, the molecular structures are depicted as orientated flat with respect to a notional surface. The effect of an upright molecular species is essentially to interchange the grazing and normal spectra, as seen in the case of Cu(BTA)$_2$ species, where spectra for both flat-lying and upright species are shown. Although in the calculations the interaction with the Au(111) substrate has been neglected, therefore essentially gas phase calculations have been performed, the calculated spectra are in good agreement with the experimental ones. In particular the spectra calculated for the hydrogen-bonded polymer (figure 5a, structure in figure 5e), are in excellent agreement with the experimental ones ([14], S2, figure SI4d), thus validating the assumption of a weak interaction with the substrate for the calculations. Optimised geometries are reported in ESI S4 and

the analysis of nitrogen atoms and respective excitations is listed in ESI (S5).

For the flat-lying hydrogen-bonded BTAH polymer, π* resonances show four peaks at 399.9, 400.5, 401.6 and 402.6 eV. The spectra and the structure of the flat-lying –[Cu(BTA)]$_n$– species is shown in figure 5b and 5f respectively. Copper atoms are bound to nitrogen atoms in the N_1 (N_3) and N'_1 (N'_3) positions and BTA moieties alternate sides along the chain. From the conformational similarity between the hydrogen-bonded and –[Cu(BTA)]$_n$– polymers, one might think that there would not be a drastic change in the nitrogen spectra. However, the calculated spectra show marked differences due to the changes in the electronic structure going from a hydrogen bonding interaction to a chemical bond between nitrogen atoms and copper. For –[Cu(BTA)]$_n$–, figure 5b, at grazing incidence at least three discernible peaks in the π* resonance are seen (400.4, 402.2 and 403.6 eV), compared to four for the hydrogen-bonded polymer, figure 5a. In fact, in the hydrogen-bonded polymer the three nitrogen atoms have inequivalent environments, whereas in –[Cu(BTA)]$_n$– there are only two, as N_1 and N_3 position are equivalent. The two Cu-N bonds in –[Cu(BTA)]$_n$– are expected to have the same chemical nature and length. Thus, one would expect a simpler spectrum for the more symmetric case of –[Cu(BTA)]$_n$–, when compared to that of hydrogen-bonded BTAH. Calculated spectra for a $Cu(BTA)_2$ species assumed upright or flat-lying are shown in figure 5c ($5c_u$ upright, $5c_f$ flat-lying) and its structure is shown in figure 5g. This case illustrates well the changes in the π* and σ* resonances with the direction of the electric vector. Four peaks are seen in the π* region, at 399.8, 400.3 eV, 401.5 and 403.3 eV. The spectra of Cu(BTA) with copper bound to either N_1 or N_2 are shown in figure 5d and their corresponding structures are reported in figure 5h. The spectrum of the monomer with the copper atom bonded to N_1 shows four distinctive peaks at 398.8, 400.3, 401.6 and 402.6 eV. The spectrum of the monomer with copper bonded to N_2, on account of its higher symmetry, shows only three peaks, at 399.7, 401.4 and 403.5 eV.

The photon energy scales of the calculated spectra of the two polymers, hydrogen-bonded and –[Cu(BTA)]$_n$–, and $Cu(BTA)_2$ species are shifted by -1.2 eV for comparison with the experimental ones, whereas for the spectra of the monomers a shift of close to -2.0 eV is required.

2.3 Discussion

Several experimental [9-14, 19-21, 38, 50-63] and computational [2-8, 11, 15-17, 22, 23] studies have set to explore the complexity of the chemistry and morphology of the species produced upon adsorption of benzotriazole on copper surfaces, focusing on the role of the specific local morphology of the surface [4, 15, 16] and in particular of copper adatoms [2, 7, 8, 11].

On a pristine Cu(111) surface, at low coverage, BTAH adsorbs dissociatively in the form of upright $Cu(BTA)_2$ and Cu(BTA) species [9]. Highly-packed self-assembled structures, essentially based upon the same species, are produced at saturation coverage and above [10]. Later, a coverage dependent combination of $Cu(BTA)_2$ and Cu-BTA chains was reported [11]. On Cu(110) adsorption is reported to occur in the form of flat-lying molecules in a $c(4 \times 2)$ configuration [12, 13]. On Cu(100), at submonolayer coverage, benzotriazole has been shown to adsorb with its molecular plane within 15° of the surface normal; at multilayer coverage, the molecular plane has been reported to tilt by ca. 40° from the plane of the substrate instead [19]. On polycrystalline copper in the form of evaporated films exhibiting predominantly {111} facets, Fang *et al.* [21] proposed a structure of upright BTA molecules connected by intramolecular hydrogen bonds between adjacent benzene and triazole rings and having an alternate tilt of 9° from the surface normal. However, inherent to such investigations and typical of UHV studies, the metal single crystal approach is complicated by the difficulty in isolating the role of the atoms belonging to the surface plane from that due to adatoms. For example, the identification of a signal due to copper adatoms under the Cu $2p_{3/2}$ peak via photoelectron spectroscopy is challenging, due to its almost negligible intensity [11]. However, copper adatoms have been shown to influence greatly the adsorption geometries of adsorbates [24, 25]. A further hurdle is to determine unambiguously the local oxidation state of copper on a copper single crystal because of the similarity of the binding energy values for copper 0 and I [43-45].

In this context, the use of copper doped Au(111) surfaces can be a convenient choice in order to isolate the behaviour of copper adatoms from the contribution due to the copper surface atoms. In fact, on such surfaces, Au(111) acts as a mere 2D support with copper-rich islands acting as a source of reactive copper atoms. This is facilitated by a multi-technique approach. The behaviour of the Cu/Au(111) system [26, 27, 29, 31, 46-48], the adsorption of BTAH on copper single crystals [9, 10, 12, 13, 19] and on Au(111) [14] have been investigated separately elsewhere.

In the present study, STM measurements show that starting from a relatively low coverage in copper, ca. 0.2 ML, and saturation of BTAH, a range of metal organic features, generally as $Cu_x(BTA)_y$ species, form and evolve as a function of the annealing temperature. The topographic measurements reported in figure 1 give some indication on the possible structures of such $Cu_x(BTA)_y$ species: they may be represented by small clusters (figure 1a) or short polymers (figure 1d), which may find some correspondence to metal-organic compounds synthesised from solution. In such clusters BTA units are expected to have their molecular planes orientated to different angles with respect to the surface. HREELS measurements (figure 2) show that upon adsorption at room temperature the amount of BTAH in excess with respect to copper adsorbs forming hydrogen-bonded chains, as on clean Au(111) [14]. In the present case, the imaging of such flat-lying, fast diffusing species is beyond the capability of STM at room temperature. Upon annealing, physisorbed species are removed. The vibrational spectra can be interpreted as indicating that a mix of flat-lying and more upright species is present (figure 2c). This is

consistent with the information derived from STM and NEXAFS. However, although STM images give some indications as to their potential structures, a chemical characterisation is still elusive.

One crucial piece of information is supplied by PES (figure 3). Upon adsorption on pristine Au(111) copper is in its metallic state, and its electronic configuration changes on reaction with BTAH in favour of a more oxidised species. Even though the Cu $2p_{3/2}$ core level peak has a narrow fwhm, a full interpretation is rather difficult. This is due to the complex structure of the top layers of the Cu/Au(111) system [26, 27, 29, 32, 46-48] and the difficulty in detecting postulated copper adatoms [11]. The absence of secondary peaks above the one observed and satellite structures allows one to exclude structural models involving Cu(II) [59]. Many studies focussing on solution chemistry report the presence of Cu(I)-BTA compounds [5, 38, 53, 56-58]. Often the presence of Cu(II) in those samples has been attributed to post oxidation due to exposure to atmosphere [60-63].

A model based on a $Cu(BTA)_2$ species, as in figure 5g, further coordinated to copper atoms through N_2 and N'_2 can explain the observation of two chemical environments for the nitrogen atoms as determined by PES: there would be a Cu-N environment (for N_1, N_2 and N'_1, N'_2) and one N-N environment (for N_3 and N'_3); the ratio would be $Cu\text{-}N_1(N_2):N_3$ = 2:1, the opposite of what is seen on Au(111) [14], where the environments and ratios are $N_1(N_3):N_2$ = 2:1. This structure would bare similarities with the $Cu_6(BTA)_4$ cluster proposed by Salorinne *et al.* [34] and is not too dissimilar from the oligomer prepared by Liu and co-workers [36]. Both previous structures would have to adopt a modified geometrical structure in order to be accommodated on a surface. For hypothetical hydrogen-bonded chains adsorbing flat on Cu(111), three nitrogen environments have been reported: one involved in a hydrogen bond (N_3, with reference to figure 5e), the central one, N_2, coordinated with a surface copper atom in a N–Cu bond and one, N_1, bonded to the hydrogen atom. Their calculated binding energies differ by ca. 0.6 eV [11, ‡]. Even though no strong chemical bonding to the surface was inferred, also on Au(111), the three nitrogen atoms are chemically different. Yet, upon adsorption the binding energies of N_1 and N_3 are perhaps very similar, so that their individual contributions are not resolved and a doublet is observed instead [14]. It is worth noting that the N 1s binding energy range calculated in [11] spans up to 4 eV depending on the chemical environment and the chemical species present. In the present work, the N 1s peaks are constant in position, indicating that the chemical environments of the nitrogen atoms do not vary much upon annealing.

The intensity of the Cu $2p_{3/2}$ peak after dosing BTAH decreases by ca. 6%, after annealing to 400 K increases by ca. 22%, then after annealing to 500 K decrease by ca. 20% and after annealing to 670 K the signal disappears completely. The N 1s and C 1s peaks show similar intensities trends with annealing: after annealing to 400 K the N 1s decreases by ca. 43%, the C 1s decreases by ca. 44.4%; after annealing to 500 K, the N 1s peak decreases by ca. 25%, the C 1s decreases by ca. 23%; after annealing to 670 K, the N 1s peak vanishes and only a residual C 1s signal is recorded.

The changes in the intensities of the photoemission signals can be rationalised as follows: after dosing to saturation, benzotriazole covers the whole surface (i.e. both the pristine Au(111) and the copper-rich islands), leading to an attenuation of the copper signal. With annealing to 400 K, physisorbed species are desorbed and there is some surface segregation of copper atoms induced by the reaction with BTA; as a consequence of both effects, the copper signal increases. Upon annealing to 500 K, desorption of some $Cu_x(BTA)_y$ species and incorporation of copper in the bulk Au(111) are competitive. Finally, after annealing to 670 K, also the remaining $Cu_x(BTA)_y$ species desorb and the remaining copper is lost to the bulk gold. From the similarity in the relative percentage decrease and the retention of the spectra profiles of the N 1s and C 1s signals, some desorption occurs, likely in the form of $Cu_x(BTA)_y$ species [10, 18, 34], with BTA moieties remaining intact on the surface after each annealing step, except the final. Decomposition of the species remaining on the surface would show as a change of the shape of the photoemission peaks [11] and presumably a loss of the NEXAFS π* structure. However, a small amount of decomposition may occur above 500 K, as suggested by the residual C 1s signal, still present after annealing to 670 K.

From the values reported in table 3, it can be observed that the N:C ratio calculated from PES is almost constant, 1:2.5, and close to the expected 1:2 ratio. Additionally, from the comparison between figures 4 and 5, the experimental π* system signatures observed via NEXAFS are consistent with the calculated ones, where intact BTA moieties are considered. These observations indicate that the BTA moieties remain intact throughout the experiments, there is no appreciable degradation on annealing, and further support the analysis of the angular dichroism in order to determine molecular orientation.

BTAH adsorbed on Cu/Au(111) behaves similarly to multilayer preparations on Cu(111), where the onset of the desorption of physisorbed species is observed at around 320 – 350 K [10, 11]. This is also in agreement with the desorption of physisorbed species observed on Au(111) [14]. The chemisorbed species, on the other hand, were seen to desorb as $Cu_x(BTA)_y$ at about 550 – 595 K [10]. Gattinoni and co-workers [11] reported the onset of desorption and surface assisted decomposition of a layer consisting of dissociated BTA arranged in dimers with a ca. 30% of BTA-Cu chains at a significantly lower temperature, around 430 – 450 K. As a further comparison, the onset of surface assisted decomposition on Ni(111) was observed at 600 K [18].

NEXAFS measurements (figure 4) and their rationalisation through comparison with the literature [11, 19], our own modelling (figure 5) and the other experimental results allow us to determine that the majority of the structures prepared upon reaction of BTAH with copper-rich islands are likely $Cu(BTA)_2$ species associated with small copper clusters, which evolve to short polymers, likely based on $[Cu(BTA)]_n$ species, upon high temperature annealing.

When considering the as prepared experimental spectrum at 20° (figure 4a), the comparison with the calculated spectra

indicates the possibility that there could be a mixture of both types of polymers (H- bonded and Cu-bonded), as the main π* peaks (400.5 eV) overlap significantly. In addition, the presence of other species cannot be ruled out *a priori*. The principal spectral signature appears to be related to the hydrogen-bonded polymer, as also suggested by the decrease in the photoelectron Cu:N peak ratio upon annealing to 400 K (table 3). On the 90° spectrum, a small π* signal bears a signature similar to that of an upright $Cu(BTA)_2$ species. Overall, when considering the information derived from STM (figure 1a), HREELS (figure 2a), PES (figure 3c), the species present are considered to consist mainly of a flat-lying hydrogen-bonded polymeric physisorbed species, as a majority, and a small amount of $Cu_x(BTA)_y$ chemisorbed species orientated more upright.

NEXAFS measurement on multilayers of BTAH on Cu(100) have reported that BTAH may adsorb in a tilted geometry characterised by an overall 40° tilt angle of the molecular plane with respect to the surface [19]. Such an overall tilt angle could also be derived from an adsorption configuration in which the top few layers are composed of flat-lying molecules, over an upright monolayer, as in the low coverage regime, which shows the opposite dichroism [19]. The dissociatively chemisorbed molecules also show a much less resolved fine structure for the π* resonance [19], as is also the case for the high coverage regime on Cu(111), which was ascribed to BTA mostly arranged in $Cu(BTA)_2$ species and partially as chains of alternating upright and flat BTA molecules [11]. The identification of $Cu(BTA)_2$ species chemisorbed upright and further coordinated with near surface copper atoms is consistent with previous STM and vibrational spectroscopy measurements on Cu(111) [9, 10].

As highlighted, on annealing to 400 K (figure 4b), the NEXAFS spectra lose the signature of the hydrogen-bonded polymer and assume something more akin to a species coordinated to copper. As for the as prepared spectra, because of the overlaps of the π* resonances for $–[Cu(BTA)]_n–$ and $Cu(BTA)_2$, both such species could be present after annealing to 400 K. A component of the copper monomers could also be present; however the assignment to a $Cu(BTA)_2$ species explains the spectral change well and also reproduces better the low energy shoulder at 403.3 eV seen in the first peak. Also different shifts in energy for both monomers and $Cu(BTA)_2$ would be required. Inclusion of the monomers would lead to a much more prominent first peak rather than a shoulder, given the presence of a feature at 398 eV. From a direct comparison between experimental and calculated spectra, it cannot be determined whether only a single species tilted to a specific angle is present, or if there is a mixture of both flat and upright species, as the NEXAFS cannot discriminate between the two configurations. A combination of the calculated spectra for the $–[Cu(BTA)]_n–$ and $Cu(BTA)_2$, adsorbed to different angles, may well explain the angular dependency of the experimental spectra, even though the morphologies of the features present on the surface are more complex than the calculated models, as derived from the STM measurements reported in figure 1. STM images show that at this temperature the prevalent condensed species is an adsorbed species similar to that shown in the inset of figure 1a.

Such structures may be composed of several $Cu(BTA)_2$ species, coordinated to a copper cluster. Because such structures are not isolated $Cu(BTA)_2$ species *per se*, they inherently bear a signature of further coordinated $Cu_x(BTA)_y$, perhaps polymeric species, albeit very short. Note that y/x evolves from 2 towards 1 with increasing length. Recently, in the low coverage adsorption of benzotriazole on Cu(111), Cu-BTA chains, in which the BTA moieties are alternating upright and flat-lying, have been reported to be the prevalent species, along with a 25-35% of upright bidentate monomers [11]. This is only partially consistent with previous low coverage STM studies, which revealed the surface to be covered in laterally stacked and diffusing $Cu(BTA)_2$ species and strongly adsorbed Cu(BTA) species [9], which have been later ascribed to the interaction of BTA with copper adatoms on the Cu(111) surface [8].

On annealing to 500 K (figure 4c) a further small desorption of $Cu_x(BTA)_y$ species from the surface is determined. However only a small variation in the dichroism is seen, as shown by the evaluation of the average angles of the π* systems (figures 4b and 4c). STM images show the appearance of a different species on the Au(111) terraces, interpreted as a $Cu_x(BTA)_y$ short polymer, with stoichiometry close to 1:1, in which some of the BTA molecules are upright, some other more tilted, and some species are anchored at steps and islands edges (figure 1d). The morphology of such a species is consistent with the NEXAFS measurements.

Recently Gattinoni and co-workers [11] have presented calculated NEXAFS spectra for various BTAH/BTA-Cu species adsorbed on Cu(111). When compared to our work, the main differences are that ours are gas-phase calculations, the methods used are different and some of the chemical species, although having the same empirical chemical formula, have different geometry. Nevertheless, there are some similarities, which are of a help in rationalising the experimental spectra.

Qualitatively our calculated spectra of the hydrogen-bonded BTAH polymer match very well with the experimental spectra recorded on Au(111), as shown in ESI S2. In ref. [11] the spectra of a flat-lying hydrogen-bonded polymer on Cu(111) are calculated instead. The main difference in the interpretation of the spectra is that those of ref. [11] involve a N_2-M (M, metal) bond [‡]. There is no evidence of a N_2-Au bond in the case of Au(111), suggesting that at least one of the nitrogen chemical environments is different from those on the study on Au(111) [14]. In addition, to date there is no experimental evidence for hydrogen-bonded flat-lying chains on Cu(111) [9, 10]. Nevertheless, the calculated spectra reported in ref. [11] are qualitatively similar to those presented in this work.

Our $–[Cu(BTA)]_n-$ chain calculated spectra could be considered similar to those obtained for the low/high coverage chains presented by ref. [11]: the π* resonances show two evident transitions and a smaller one. However, the geometries are notably different: the models proposed by Gattinoni *et al.* [11] show alternation of upright and tilted BTA moieties coordinated to the Cu(111) surface through adatoms, whereas our model is just a flat structure with BTA moieties alternating either side. It is argued that the different orientation of the BTA moieties

would result in a difference in the dichroism, which is not observed here.

It is difficult to compare the spectra calculated for the $Cu(BTA)_2$ species: although the chemical species are similar, differences in the chemical environments of the nitrogen atoms arise when considering the bonding with the surface. In our gas phase model only the $N_1(N'_1)$-Cu bond is present; the model proposed in ref. [11] takes into account also the interaction with the surface through $N_2(N'_2)$, whereas N_3 (N'_3) is bound to an adatom [‡].

No direct comparison can be made between the calculated spectra of the monomers in this work and that of ref. [11], as ours are monosubstituted, whereas that of ref. [11] is adsorbed upright through N_1 and N_3 [‡].

The most significant changes occurring upon depositing copper, followed by BTAH, and after annealing, are highlighted in scheme 2: on clean Au(111) (scheme 2a), copper is added, as evidenced by the appearance of Cu-rich features (scheme 2b); after exposure to BTAH, preferential chemisorption thorough the triazole moiety occurs on Cu-rich areas; physisorption as hydrogen-bonded chains is seen on the unmodified Au(111) surface (scheme 2c); annealing to ca. 400 K causes desorption of the hydrogen-bonded physisorbed and induces copper migrating into the bulk gold, whereas chemisorbed species still remain anchored to the surface in various orientations (scheme 2d); upon annealing to ca. 500 K part of the chemisorbed species desorb, part reorganise in short polymers initiated at step (or islands) edges; copper keeps migrating into the bulk gold (scheme 2e); finally, as a consequence of annealing to 650 K, all molecular features are desorbed, copper has fully dissolved into the bulk gold and the morphology of Au(111) surface is slightly changed, with the appearance of a gold island where a Cu-rich island had formed upon deposition of copper (scheme 2f).

The identification of the $Cu(BTA)_2$ as a prevalent species, accompanied by short oligomers, is in agreement with several recent studies [9-11]. The reason why the necklace polymer, although calculated to be the most energetically favourable structure [3, 8, 11, 15, 23] is elusive has yet to be understood, but is likely linked to the amount and character of copper atoms available.

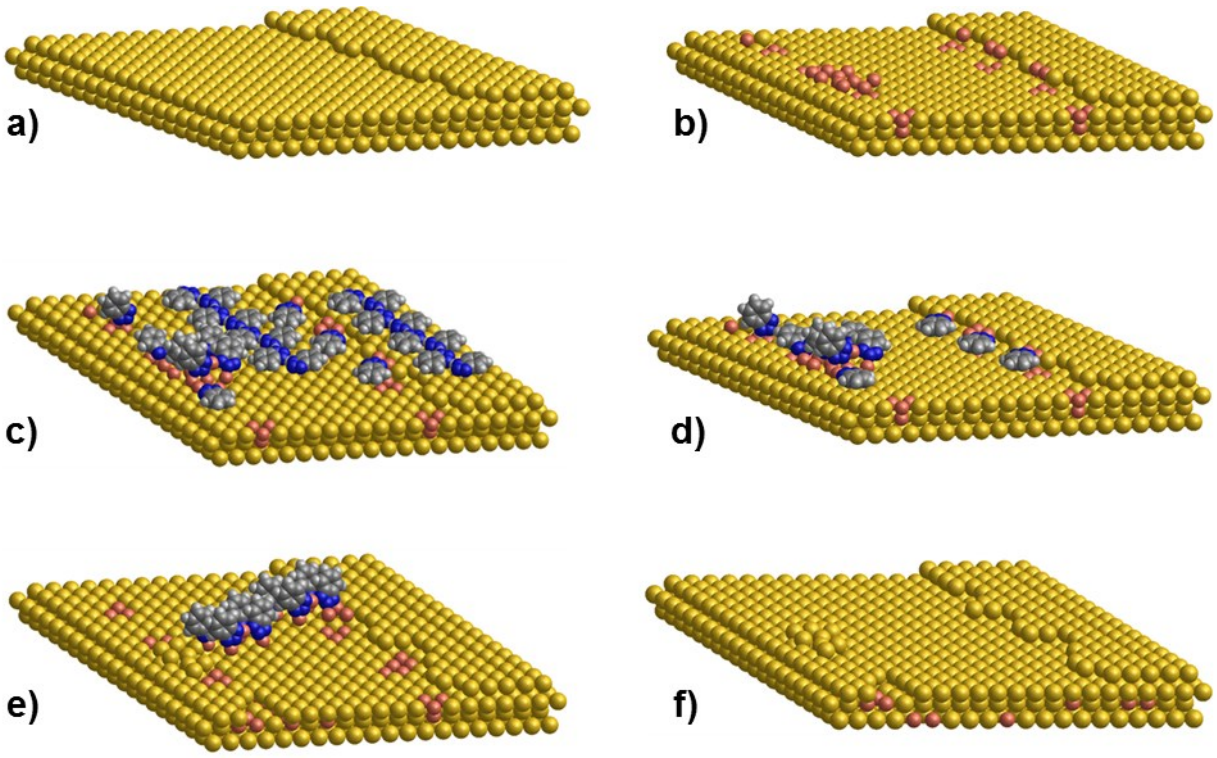

Scheme 2. Most significant changes occurring upon depositing copper, followed by BTAH, and after annealing. a) clean Au(111); b) addition of Cu; c) addition of BTAH; d) annealing to 400 K; e) annealing to 500 K; f) annealing to 650 K; see text for detailed description. Colour scheme: H, light grey; C, dark grey; N, blue; Cu, orange; Au, yellow.

3. Experimental and computational details

The Au(111) single crystal was cleaned by argon ion sputtering at room temperature and annealing (ca. 830 K) cycles until a surface characterized by the typical (22 × √3) structure of the reconstructed clean substrate was observed by both LEED and STM. BTAH dosing was carried out by opening a gate valve separating a quartz crucible containing the compound from the main chamber containing the Au(111) crystal held at room temperature. BTAH has a vapour pressure high enough at room temperature to sublime under UHV conditions [20]. Copper was dosed on the Au(111) surface by electrically heating a high purity copper wire wrapped around a tantalum filament, yielding a deposition rate of ca. 0.07 ML min^{-1} [26, 27]. The copper coverage was calibrated by following the decrease of the Au $4f_{7/2}$ surface component on photoemission spectra.

HREELS (VSW HIB 1001 double-pass spectrometer) measurements were carried out in a UHV system with a base pressure better than 1×10^{-10} mbar, in the specular direction ($\theta_i = \theta_f = 45°$), with a primary beam energy of 4 eV and a typical elastic peak resolution of ca. 50 cm^{-1} (6.2 meV fwhm). STM (VT-STM Omicron) experiments were performed scanning in constant current mode, using home-made, electrochemically etched, tungsten tips. Images were processed using the WSxM software package [64].

NEXAFS and photoemission measurements were performed at the SuperESCA beamline [65, 66] of the Elettra third generation synchrotron radiation source in Trieste, Italy. The experimental chamber was equipped with a Phoibos hemispherical energy analyzer (SPECS GmbH) with a homemade delay-line detector [67] and had a background pressure of about 2×10^{-10} mbar. NEXAFS data were collected by monitoring the yield of N KLL Auger electrons at 380 eV. Data were recorded for angles of incidence in the range $20° \leq \theta \leq 90°$; the angle between the photon beam and the electron energy analyser was 70° and the linear polarisation ca. 100%. Data were normalised following an established procedure that includes dividing the spectrum of the adsorbate covered surface by that of the clean surface [68], having first divided each spectrum by the measured incident photon flux as recorded from a clean gold mesh located close to the main experimental chamber. Normalisation to a unit step height and peak fitting were done using the Athena package [69]. Angular dependency and estimation of the orientation of the molecular plane were addressed according to [54, 68].

Core level photoemission spectra were recorded with the sample at room temperature and at photon energies of 320 eV (Au 4f), 400 eV (C 1s), 500 eV (N 1s), or 1050 eV (Cu $2p_{3/2}$) with an overall energy resolution better than 100 meV at a photon energy of 320 eV and 250 meV at a photon energy of 1050 eV. At these photon energies the kinetic energies for emission from each of the elemental core levels are of ca. 100 eV for all spectra; therefore the transmission function of the analyser can be considered constant for all measurements. Binding energies were referenced to the Fermi level recorded for each photon energy. Photoemission spectra were used to verify surface cleanliness. Damage to the overlayer was minimized by probing the sample at different surface locations for each measurement. Data fitting was done using the CasaXPS software [70]; in the quantitative determination of the stoichiometric ratios, the following cross-sections were used (in the dipole length approximation, referenced to C 1s): C 1s 1, N 1s 0.925, Cu $2p_{3/2}$ 1.210 [71, 72]. Spectra were normalised by dividing the measured signal by the number of scans and the photon flux.

Density Functional Theory (DFT) calculations for both the geometry optimisation and the NEXAFS spectra at the N-edge for several benzotriazole, and benzotriazole-copper related species were performed using the StoBe code [55, 73]. The non-local exchange functional of Becke [74], together with the correlation functional of Perdew [75], were used for the density functional. For the ground state calculations, TZVP basis sets [76] were used: 7111/411/1 for carbon and nitrogen and 311/1 for hydrogen together with the auxiliary basis sets of (5,2; 5,2) for carbon and nitrogen and (3,1; 3,1) for hydrogen. For the excited state NEXAFS spectra, the half core hole approach, or transition state approach, was applied [77, 78]; this approach is considered as a balance between initial and final state effects and includes relaxation terms. Apart from this treatment of the relaxation, the calculation does not include any other treatment of processes that are on the time scale of the lifetime of the core hole and could affect the resonance intensity and structure. No bonding to the Au(111) surface is considered, in the assumption of a weak interaction with the substrate [14]; the geometrical structures are from optimised “gas phase” species.

4. Conclusions

The formation and thermal behaviour of low dimensional metal organic species produced upon adsorption of benzotriazole on copper-doped Au(111) surfaces have been investigated through complementary surface sensitive techniques and supported by computational modelling. Benzotriazole has been seen to physisorb as a hydrogen-bonded species on unmodified Au(111), whereas on copper-rich areas dissociative chemisorption occurs. The prevalent species is a $Cu(BTA)_2$ metal organic compound further coordinated with copper atoms on or in the gold surface top layers. Short polymers (oligomers) based on a Cu:BTA 1:2 ratio are also seen. On annealing such oligomers evolve into longer polymers, with a ratio moving in favour of 1:1; however, the necklace polymer, which is considered the most stable structure formed on adsorption of BTAH on copper surfaces, was not observed. The tendency to produce oligomers, rather than extended polymers, may be linked to the limited availability of active copper atoms.

These findings contribute to a further understanding of the interaction between benzotriazole and copper and, in turn, are expected to help in rationalizing the mechanism at the basis of the protection of copper and copper alloys from corrosive phenomena.

Conflicts of interest

There are no conflicts to declare.

Acknowledgements

FG has received funding from the European Community's Seventh Framework Programme (FP7/2007-2013) under grant agreement nº 312284 for part of the research leading to these results (NEXAFS, photoelectron spectroscopy). The Engineering and Physical Sciences Research Council (EPSRC) is acknowledged for the funding of CRL's PhD studentship (EP/M506631/1). Prof. Christopher J. Baddeley (University of St Andrews) and Dr. Silvano Lizzit (SuperESCA beam line, Elettra) are thanked for fruitful discussions.

The research data underpinning this publication can be accessed at https://doi.org/10.17630/e7e316c9-abd5-4814-a9c1-a5929718b419 (will be activated upon acceptance).

Notes and references

‡ The difference between the present work and ref. [11] in numbering the nitrogen atoms is here highlighted.

1 M. Finšgar and I. Milošev, Corr. Sci., 2010, 52, 2737.
2 A. Kokalj and S. Peljhan, Langmuir, 2010, 26, 14582.
3 A. Kokalj, S. Peljhan, M. Finšgar and I. Milošev, J. Am. Chem. Soc., 2010, 132, 16657.
4 S. Peljhan and A. Kokalj, Phys. Chem. Chem. Phys., 2011, 13, 20408.
5 L. Cohen, V. A. Brusic, F. B. Kaufman, G. S. Frankel, S. Motakef and B. M. Rush, J. Vac. Sci. Technol. A., 1990, 8, 2417.
6 Y. Jiang and J. B. Adams, Surf. Sci., 2003, 529, 428.
7 X. Chen and H. Häkkinen, J. Phys. Chem. C, 2012, 116, 22346.
8 C. Gattinoni and A. Michaelides, Faraday Discuss., 2015, 180, 439.
9 F. Grillo, D. W. Tee, S. M. Francis, H. Früchtl and N. V. Richardson, Nanoscale, 2013, 5, 5269.
10 F. Grillo, D. W. Tee, S. M. Francis, H. A. Früchtl and N. V. Richardson, J. Phys. Chem. C, 2014, 118, 8667.
11 C. Gattinoni, P. Tsaousis, C. Euaruksakul, R. Price, D. A. Duncan, T. Pascal, D. Prendergast, G. Held and A. Michaelides, Langmuir, 2019, 35, 4, 882.
12 K. Cho, J. Kishimoto, T. Hashizume and T. Sakurai, Jpn. J. Appl. Phys., 1994, 33, L125.
13 K. Cho, J. Kishimoto, T. Hashizume, H. W. Pickering and T. Sakurai, Appl. Surf. Sci., 1995, 87-88, 380.
14 F. Grillo, J. A. Garrido Torres, M.-J. Treanor, C. R. Larrea, J. P. Götze, P. Lacovig, H. A. Früchtl, R. Schaub and N. V. Richardson, Nanoscale, 2016, 8, 9167.
15 S. Peljhan, J. Koller and A. Kokalj, J. Phys. Chem. C, 2014, 118, 933.
16 S. Peljhan, J. Koller and A. Kokalj, J. Phys. Chem. C, 2014, 118, 944.
17 N. Kovačević and A. Kokalj, Materials Chem. Phys., 2012, 137, 331.
18 C. C. Chusuei, J. V. de la Peña and J. A. Schreifels, Rev. Sci. Instrum., 1999, 70, 3719.
19 J. F. Walsh, H. S. Dhariwal, A. Gutierrez-Sosa, P. Finetti, C. A. Muryn, N. B. Brookes, R. J. Oldman, and G. Thornton, Surf. Sci., 1998, 415, 423.
20 Y. Park, H. Noh, Y. Kuk, K. Cho and T. Sakurai, J. Korean Phys. Soc., 1996, 29, 745.
21 B. –S. Fang, C. G. Olson and D. W. Linch, Surf. Sci., 1986, 176, 476.
22 A. Kokalj, N. Kovačević, S. Peljhan, M. Finšgar, A. Lesar and I. Milošev, ChemPhysChem, 2011, 12, 3547.
23 A. Kokalj, Faraday Discuss., 2015, 180, 415.
24 Q. Chen, C. C. Perry, B. G. Frederick, P. W. Murray, S. Haq and N. V. Richardson, Surf. Sci., 2000, 446, 63.
25 F. M. Leibsle, S. Haq, B. G. Frederick, M. Bowker and N. V. Richardson, Surf. Sci., 1995, 343, L1175.
26 F. Grillo, H. Früchtl, S. M. Francis and N. V. Richardson, N. J. Phys., 2011, 13, 013044.
27 F. Grillo, R. Megginson, J. Christie, S. M. Francis, N. V. Richardson and C. J. Baddeley, eJ. Surf. Sci. Nanotech., 2018, 16, 163.
28 F. Grillo, H. Früchtl, S. M. Francis, V. Mugnaini, M. Oliveros, J. Veciana and N. V. Richardosn, Nanoscale, 2012, 4, 6718.
29 L. Wang, P. Li, H. Shi, Z. Li, K. Wu and X. Shao, J. Phys. Chem. C, 2017, 121, 7977.
30 T. Lin, X. S. Shang, J. Adisoejoso, P. N. Liu and N. Lin, J. Am. Chem. Soc., 2013, 135, 3576.
31 J. Liu, T. Lin, Z. Shi, F. Xia, L. Dong, P. N. Liu and N. Lin, J. Am. Chem. Soc., 2011, 133, 18760.
32 X. Zhao, P. Liu, J. Hrbek, J. A. Rodriguez and M. Pérez, Surf. Sci., 2005, 592, 25.
33 X. Zhao and J. Rodriguez, Surf. Sci., 2006, 600, 2113.
34 K. Salorinne, X. Chen, R. W. Troff, M. Nissinen and H. Häkkinen, Nanoscale, 2012, 4, 4095.
35 T. Trimble, L. Tang, N. Vasiljevic, N. Dimitrov, M. van Schilfgaarde, C. Friesen, C. V. Thompson, S. C. Seel, J. A. Floro and K. Sieradzki, Phys. Rev. Lett., 2005, 92, 166106.
36 J.-J. Liu, Z.-Y. Li, X. Yuan, Y. Wang and C.-C. Huang, Acta Cryst., 2014, C70, 599.
37 W. Roth, D. Spangenberg, Ch. Janzen, A. Westphal and M. Schmitt, Chemical Physics, 1999, 248, 17.
38 J. Rubim, I. G. R.Gutz, O. Sala and W. J. Orville-Thomas, J. Molecular Structure, 1983, 100, 571.
39 I. Popova and J. T. Yates Jr., Langmuir, 1997, 13, 6169.
40 L. F. Peña, J.-F. Veyan, M. A. Todd, A. Derecskei-Kovacs and Y. J. Chabal, ACS Appl. Mater. Interfaces, 2018, 10, 38610.
41 C. Toernkvist, J. Bergman, and B. Liedberg, J. Phys. Chem., 1991, 95, 3119.
42 B. Gao, B. Tan, Y. Liu, C. Wang, Y. He and Y. Huang, Surf. Interface Anal., 2019, 51, 566.
43 X-ray Photoelectron Spectroscopy Database Version 4.1, National Institute of Standards and Technology, Gaithersburg (2012) (Accessed March 2019); http://srdata.nist.gov/xps/
44 D. Tahir and S. Tougaard, J. Phys. Condens. Matter, 2012, 24, 175002.
45 C. D. Wagner, W. M. Kiggs, L. E. Davis, J. F. Moulder, *Handbook of X-ray Photoelectron Spectroscopy*; Perkin-Elmer Corporation-Physical Electronics Division, Eden Prairie, MN (1979)
46 M. Kuhnand and T. K. Sham, Phys. Rev. B, 1994, 49, 1647.
47 T. K. Sham, A. Hiraya and M. Watanabe, Phys. Rev. B, 1997, 55, 7585.
48 F. Grillo, R. Megginson, D. Batchelor, M. Muntwiler and C. J. Baddeley, Jpn. J. Appl. Phys., 2019, 58, SIIIB09.
49 A. Mezzi, E. Angelini, T. De Caro, S. Grassini, F. Faraldi, C. Riccucci and G. M. Ingo, Surf. Interface Anal., 2012, 44, 968.
50 H. G. Tompkins and S. P. Sharma, Surf. Interface Anal., 1982, 4, 261.
51 G. Xue, J. Ding, P. Lu and J. Dong, J. Phys. Chem., 1991, 95, 7380.
52 I. A. Arkhipushkin, L. I. Yesina, Yu. Ya. Andreev, L. P. Kazansky and Yu. I. Kuznetsov, Int. J. Corros. Scale Inhib., 2012, 2, 107.
53 M. Finšgar, J. Kovač and I Milošev, J. Electrochem. Soc., 2010, 157, C52.
54 J. Stöhr and D. A. Outka, Phys. Rev. B, 1987, 36, 7891.

55 D. R. Batchelor, U. Aygül, U. Dettinger, M. Ivanovic, A. Tournebize, S. Mangold, M. Forster, U. Scherf, H. Peisert and T. Chassé, European Polymer Journal, 2016, 81, 686.
56 M. Finšgar, S. Peljhan, A. Kokalj, J. Kovač and I. Milošev, J. Electrochem. Soc., 2010, 157, C295.
57 G. W. Poling, Corros. Sci., 1970, 10, 359.
58 J. B. Cotton and I. R. Scholes, Brit. Corrosion J., 1967, 2, 1.
59 G. Xue and J. Ding, Applied Surf. Sci., 1990, 40, 327.
60 R. F. Roberts, J. Electron Spectr. Rel. Phenom., 1974, 4, 273.
61 D. Chadwick and T. Hashemi, J. Electron Spectr. Rel. Phenom., 1977, 10, 79.
62 D. Chadwick and T. Hashemi, Corr. Sci., 1978, 18, 39.
63 A. Mirarco, S. M. Francis, C. J. Baddeley, A. Glisenti and F. Grillo, Corr. Sci., 2018, 143, 107.
64 I. Horcas R. Fernández, J. M. Gómez-Rodríguez, J. Colchero, J. Gómez-Herrero and A. M. Baro, Rev. Sci. Instrum., 2007, 78, 013705.
65 A. Baraldi, M. Barnaba, B. Brena, D. Cocco, G. Comelli, S. Lizzit, G. Paolucci and R. Rosei, J. Electron Spectrosc. Relat. Phenom., 1995, 76, 145.
66 A. Baraldi, G. Comelli, S. Lizzit, M. Kiskinova and G. Paolucci, Surf. Sci. Reports, 2003, 49, 169.
67 G. Cautero, R. Sergo, L. Stebel, P. Lacovig, P. Pittana, M. Predonzani and S. Carrato, Nucl. Instrum. Meth. A, 2008, 595, 447459.
68 J. Stöhr, *NEXAFS spectroscopy*, in: R. Gomer (Ed.), Spreinger Series in Surface Science, 25, Spreinger, Berlin, 1992.
69 B. Ravel and M. Newville, J. Synchrotron Radiation, 2005, 12, 537.
70 CasaXPS software version 2.3.17 (Casa Software Ltd, Teignmouth, UK).
71 J. J. Yeh, *Atomic Calculation of Photoionization Cross-Sections and Asymmetry Parameters*, Gordon and Breach Science Publishers, Langhorne, PE (USA), 1993
72 J. J. Yeh and I. Lindau, Atomic Data and Nuclear Data Tables, 1985, 32, 1.
73 StoBe-deMon, K. Hermann and L. G. M. Pettersson, M. E. Casida, C. Daul, A. Goursot, A. Koester, E. Proynov, A. St-Amant, D. R. Salahub. Contributing authors: V. Carravetta, H. Duarte, C. Friedrich, N. Godbout, M. Gruber, J. Guan, C. Jamorski, M. Leboeuf, M. Leetmaa, M. Nyberg, S. Patchkovskii, L. Pedocchi, F. Sim, L. Triguero, A. Vela. <http://www.fhi-berlin.mpg.de/KHsoftware/StoBe>.
74 A. D. Becke, Phys. Rev. A, 1988, 38, 3098.
75 J. P. Perdew and Y. Wang, Phys. Rev. B, 1986, 33, 8800.
76 N. Godbout, D. R. Salahub, J. Andzelm and E. Wimmer, Can. J. Chem., 1992, 70, 560.
77 J. C. Slater and K. H. Johnson, Phys. Rev. B, 1972, 5, 844.
78 T. C. M. Leite, A. L. F. De Barros, G. B. Ferreira, A. C. O. Guerra and C. C. Turci, Int. J. Quantum Chem., 2012, 112, 3421.